Towards Practical Reproduction of Stochastic Concept Bottleneck Models

Anonymous authors
Paper under double-blind review

Abstract

Stochastic Concept Bottleneck Models (SCBMs) model dependencies among concept logits with a joint Gaussian distribution, enabling interventions on corrected concepts to propagate to related non-intervened concepts. We reproduce the main SCBM experiments on a synthetic correlated-concept dataset and two natural image datasets, comparing SCBM with Hard CBM, autoregressive CBM, and Concept Embedding Models. Our results broadly validate the original empirical findings: SCBM remains competitive in predictive accuracy, improves concept-probability calibration, and enables more efficient interventions, requiring fewer manual concept corrections to achieve comparable concept and target accuracy. Beyond empirical reproduction, we study the practical cost of reproducing SCBM. We identify implementation bottlenecks in the official codebase and introduce a refactored, GPU-oriented pipeline with optimized data loading, batched model execution, batch-first intervention evaluation, and a vectorized Frank-Wolfe solver for dependency-aware interventions. These changes reduce the practical reproduction cost to approximately 62 wall-clock hours on a single RTX 4090. Our optimized implementation also changes the relative runtime behavior reported in the original paper, indicating that computational-efficiency claims are sensitive to implementation choices. Our study therefore supports SCBM's core methodological contribution while suggesting that its practical value should be framed primarily around dependency-aware intervention rather than raw computational efficiency.

1 Introduction

Concept Bottleneck Models (CBMs) provide an interpretable alternative to standard end-to-end neural networks by requiring predictions to be mediated through human-interpretable concepts (Koh et al., 2020; Havasi et al., 2022; Shin et al., 2023). Rather than explaining a prediction only after it has been made, CBMs expose an intermediate concept layer that users can inspect and, when necessary, correct. This test-time intervention mechanism is one of the central motivations for CBMs: if a predicted concept is wrong, replacing it with the correct value can improve the final target prediction. This makes CBMs attractive when interpretability is expected to support human oversight rather than only provide post-hoc explanations.

However, a key limitation of standard CBMs is that they typically treat concept predictions independently. As a result, correcting one concept changes only that concept and leaves the remaining concept predictions fixed, even when concepts are statistically dependent. This can make interventions inefficient when concepts are correlated. Stochastic Concept Bottleneck Models (SCBMs) (Vandenhirtz et al., 2024) address this limitation by learning a joint Gaussian distribution over the concept logits. The learned dependency structure allows interventions on corrected concepts to propagate to related non-intervened concepts. The original SCBM paper reports that this dependency-aware bottleneck improves concept-probability calibration and intervention efficiency while maintaining competitive predictive performance.

Nonetheless, reproducing these results is practically nontrivial. As estimated by Vandenhirtz et al. (2024), reproducing the full set of experiments with the original implementation requires approximately 1,200 GPU hours on GeForce RTX 2080 hardware. In our initial profiling of the official implementation, we observed low and unstable GPU utilization, with overhead arising from CPU-side data loading, training-time metric

computation, Python-loop-based model execution, and repeated CPU–GPU transfers during intervention evaluation. The original paper also discusses computational efficiency, but such runtime comparisons can be sensitive to implementation choices. This naturally leads us to investigate whether the main empirical conclusions of SCBM hold under an independent reproduction, and how its practical efficiency should be evaluated once implementation bottlenecks are addressed.

To answer these two questions, we reproduce the main SCBM experiments on a synthetic dataset and two natural image datasets. We compare SCBM with Hard CBM (Havasi et al., 2022), autoregressive CBM (Havasi et al., 2022), and Concept Embedding Models (Espinosa Zarlenga et al., 2022), evaluating predictive performance, concept-probability calibration, and intervention performance. In parallel, we refactor the official codebase and optimize the main computational bottlenecks in data loading, model execution, and intervention evaluation, including a GPU-accelerated solver for dependency-aware interventions.

Contributions Our study makes three contributions. (i) We broadly validate the main empirical claims of SCBM: SCBM remains competitive in predictive performance, improves concept-probability calibration, and enables more efficient interventions by propagating information from corrected concepts to correlated non-intervened concepts. (ii) We identify and address major implementation bottlenecks in the original experimental pipeline, substantially reducing the practical reproduction cost on modern hardware. (iii) We show that runtime comparisons are sensitive to implementation choices. Our optimized implementation changes the relative runtime behavior of the compared models, suggesting that the practical value of SCBM should be framed primarily around dependency-aware interventions rather than raw computational efficiency.

2 Related Work

CBMs (Koh et al., 2020) are typically trained on supervised data of the form $(\boldsymbol{x}, \boldsymbol{c}, y)$, where $\boldsymbol{x} \in \mathbb{R}^p$ denotes the input with p covariates, $\boldsymbol{c} \in \mathbb{R}^C$ is a concept vector of C human-interpretable concepts, and $y \in \mathbb{R}$ is the target label. A CBM factorizes prediction into a concept predictor and a target predictor, $\hat{\boldsymbol{c}} = h_\phi(\boldsymbol{x})$ and $\hat{y} = g_\psi(\hat{\boldsymbol{c}}) = g_\psi(h_\phi(\boldsymbol{x}))$, so that the final prediction is mediated by the predicted concept bottleneck.

The form of the bottleneck affects the faithfulness of the resulting concept-based explanation. In the soft CBM setting considered by Koh et al. (2020), continuous concept logits $\boldsymbol{\eta} \in \mathbb{R}^C$ are passed to the target predictor. However, subsequent work argues that continuous concept logits can encode information beyond the predefined concepts, weakening the faithfulness of the bottleneck (Margeloiu et al., 2021; Mahinpei et al., 2021). Hard CBMs (Havasi et al., 2022) mitigate this problem by passing binarized concept values $\hat{\boldsymbol{c}} \in \{0, 1\}^C$ to the target predictor, rather than continuous concept logits. Havasi et al. (2022) further use autoregressive concept predictors to capture correlations among concepts while retaining a hard bottleneck. In this model, each concept c_i is predicted by a separate MLP that takes an intermediate representation from the encoder and the previous concepts $c_1, \ldots, c_{i-1}$ as input. This allows earlier concepts to influence later concept predictions, but makes the learned dependency structure dependent on the chosen concept ordering.

Concept Embedding Models (CEMs) (Espinosa Zarlenga et al., 2022) take a different approach by representing each concept with a high-dimensional embedding rather than a single scalar. For each concept i, CEM learns positive and negative concept embeddings, denoted by $\boldsymbol{z}_i^+$ and $\boldsymbol{z}_i^-$. A learnable scoring function estimates the concept probability $\hat{p}_i$, and the concept representation is formed as $\hat{\boldsymbol{z}}_i = \hat{p}_i \boldsymbol{z}_i^+ + (1 - \hat{p}_i)\boldsymbol{z}_i^-$. The concatenation of all concept embeddings is then passed to the target predictor. CEMs therefore provide a strong embedding-based alternative to scalar concept bottlenecks, aiming to improve predictive performance while preserving concept-level interpretability.

An attractive property of CBMs is that they allow users to replace a subset of predicted concepts with corrected values and then recompute the target prediction. An intervention policy determines the order in which concepts are intervened on. This order matters because concept interventions require human effort; correcting more informative concepts earlier can therefore improve performance with fewer manual interventions. The original CBM work considers random concept interventions (Koh et al., 2020). Later work studies intervention policies that select concepts according to some criteria such as predicted uncertainty, reducing the need for users to manually search over the full concept set (Sheth et al., 2022; Shin et al., 2023). However, these intervention policies primarily decide which concepts to correct; they do not by

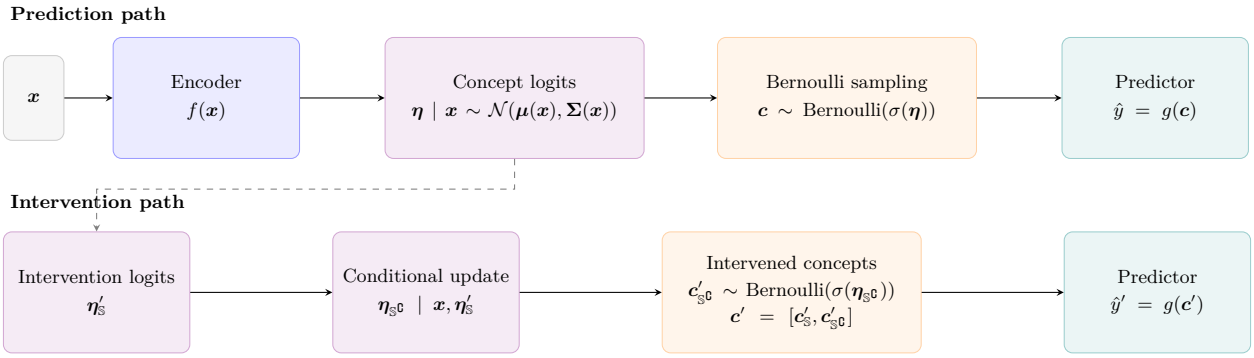

Figure 1: Overview of the SCBM framework. *Top:* During prediction, the encoder outputs a Gaussian distribution over concept logits $\boldsymbol{\eta}$, from which binary concepts $\boldsymbol{c}$ are sampled and passed to the predictor. *Bottom:* During intervention, for a set of intervened concepts $\mathbb{S}$, the corresponding concept logits $\boldsymbol{\eta}\mathbb{S}$ are altered to the intervention logits $\boldsymbol{\eta}'\mathbb{S}$, which are used to conditionally update the remaining logits $\boldsymbol{\eta}_{\mathbb{S}^\complement}$; the final prediction $\hat{y}'$ uses both the intervened true concepts and the updated non-intervened concepts.

themselves update the remaining concept predictions after an intervention. This limitation is important when concepts are statistically dependent, because correcting one concept may provide evidence about other related concepts. Autoregressive CBM (Havasi et al., 2022) partially addresses this problem by conditioning later concept predictions on earlier concepts, so an intervention on an earlier concept can affect subsequent concept predictions. However, this dependency propagation is tied to a predefined concept ordering and the imposed order may not reflect a natural semantic or causal structure. SCBM (Vandenhirtz et al., 2024) addresses this gap by learning a joint distribution over concept logits, so that interventions can propagate information to correlated concepts through the learned dependency structure without imposing a fixed autoregressive ordering.

3 Method

3.1 Model Formulation

A schematic overview of the SCBM framework is shown in Figure 1. The SCBM framework models concept dependencies by replacing deterministic concept logits with an explicit joint distribution over latent concept logits. For each input $\boldsymbol{x}$, an encoder predicts the parameters of a Gaussian distribution over concept logits $\boldsymbol{\eta} \mid \boldsymbol{x} \sim \mathcal{N}\big(\boldsymbol{\mu}(\boldsymbol{x}), \boldsymbol{\Sigma}(\boldsymbol{x})\big)$, where $\boldsymbol{\eta} \in \mathbb{R}^C$, $\boldsymbol{\mu}(\boldsymbol{x}) \in \mathbb{R}^C$, and $\boldsymbol{\Sigma}(\boldsymbol{x}) \in \mathbb{R}^{C \times C}$.

Standard CBMs typically treat concept predictions as conditionally independent given the input. SCBMs relax this assumption, where conditioned on $\boldsymbol{\eta}$, each concept is modeled independently as a Bernoulli variable:

$$p(\boldsymbol{c} \mid \boldsymbol{\eta}) = \prod_{i=1}^{C} p(c_i \mid \eta_i) = \prod_{i=1}^{C} \text{Bernoulli}\big(c_i; \sigma(\eta_i)\big).$$

The concept distribution is then trained by minimizing the negative marginal log-likelihood of the observed concepts:

$$\mathcal{L}_c = -\log p(\boldsymbol{c} \mid \boldsymbol{x}) = -\log \int p(\boldsymbol{c} \mid \boldsymbol{\eta}) p_\phi(\boldsymbol{\eta} \mid \boldsymbol{x}) d\boldsymbol{\eta}.$$

Because this integral has no closed-form solution, SCBM approximates it using M Monte Carlo samples $\boldsymbol{\eta}^{(m)} \sim \mathcal{N}(\boldsymbol{\mu}(\boldsymbol{x}), \boldsymbol{\Sigma}(\boldsymbol{x}))$. Together with the factorization of $p(\boldsymbol{c} \mid \boldsymbol{\eta})$, concept loss can be estimated as

$$\mathcal{L}_c = -\log \left(\frac{1}{M} \sum_{m=1}^{M} \exp \left[-\sum_{i=1}^{C} \text{BCE}\big(c_i, \sigma(\eta_i^{(m)})\big) \right] \right),$$

where BCE is the Binary Cross-Entropy loss and $\sigma(\cdot)$ denotes the sigmoid function. Additional details on the Monte Carlo estimators for the concept loss are provided in Appendix A.

To mitigate information leakage, SCBMs follow the approach of Hard CBMs (Havasi et al., 2022) by passing sampled binary concept values rather than continuous logits to the target predictor g_ψ. During training, the straight-through Gumbel-Softmax trick (Jang et al., 2017; Maddison et al., 2017) is applied to provide a differentiable approximation for the discrete Bernoulli sampling. The target predictor is optimized by minimizing the negative log-likelihood of the target label y given the sampled concepts:

$$\mathcal{L}_y \approx -\log\left(\frac{1}{M}\sum_{m=1}^{M} p_\psi(y \mid \boldsymbol{c}^{(m)})\right) = \mathrm{CE}\left(y,\, \frac{1}{M}\sum_{m=1}^{M} g_\psi(\boldsymbol{c}^{(m)})\right),$$

where $\boldsymbol{c}^{(m)} \sim \mathrm{Bernoulli}\big(\sigma(\boldsymbol{\eta}^{(m)})\big)$, $\boldsymbol{\eta}^{(m)} \sim \mathcal{N}(\boldsymbol{\mu}(\boldsymbol{x}),\, \boldsymbol{\Sigma}(\boldsymbol{x}))$, and CE denotes the Cross-Entropy loss.

Finally, SCBMs regularize the learned dependency structure by penalizing the off-diagonal entries of the precision matrix, following the graphical-lasso intuition (Friedman et al., 2008):

$$\mathcal{L}_{\mathrm{reg}} = \sum_{i \neq j} \left| \left[\boldsymbol{\Sigma}_\phi(\boldsymbol{x})^{-1}\right]_{ij} \right|.$$

The final training objective is

$$\mathcal{L} = \mathcal{L}_c + \lambda_y \mathcal{L}_y + \lambda_{\mathrm{reg}} \mathcal{L}_{\mathrm{reg}},$$

where λ_y and λ_{reg} control the relative weights of the target loss and the precision-matrix regularization.

3.2 Dependency-Aware Interventions

A key advantage of CBMs is that they support test-time interventions: when a user identifies an incorrectly predicted concept, the concept value can be replaced with a corrected value before recomputing the target prediction. In a standard CBM (Koh et al., 2020), intervening on one concept only changes that concept and leaves the remaining concept predictions fixed. This can make intervention inefficient when concepts are correlated. SCBMs address this limitation by updating the non-intervened concepts via the learned joint Gaussian distribution over concept logits. Let $\mathbb{S} \subset \{1, \ldots, C\}$ denote the set of intervened concepts and let $\mathbb{S}^{\complement}$ denote its complement. Given intervention logits $\boldsymbol{\eta}'_{\mathbb{S}}$ for the corrected concepts, the logits of the non-intervened concepts $\boldsymbol{\eta}_{\mathbb{S}^{\complement}}$ can be updated by conditioning the learned Gaussian distribution:

$$\begin{aligned}
\boldsymbol{\eta}_{\mathbb{S}^{\complement}} \mid \boldsymbol{x}, \boldsymbol{\eta}'_{\mathbb{S}} &\sim \mathcal{N}\left(\bar{\boldsymbol{\mu}}_{\mathbb{S}^{\complement}}, \overline{\boldsymbol{\Sigma}}_{\mathbb{S}^{\complement}\mathbb{S}^{\complement}}\right), \\
\bar{\boldsymbol{\mu}}_{\mathbb{S}^{\complement}} &= \boldsymbol{\mu}_{\mathbb{S}^{\complement}} + \boldsymbol{\Sigma}_{\mathbb{S}^{\complement},\mathbb{S}} \boldsymbol{\Sigma}_{\mathbb{S},\mathbb{S}}^{-1} (\boldsymbol{\eta}'_{\mathbb{S}} - \boldsymbol{\mu}_{\mathbb{S}}), \\
\overline{\boldsymbol{\Sigma}}_{\mathbb{S}^{\complement}\mathbb{S}^{\complement}} &= \boldsymbol{\Sigma}_{\mathbb{S}^{\complement},\mathbb{S}^{\complement}} - \boldsymbol{\Sigma}_{\mathbb{S}^{\complement},\mathbb{S}} \boldsymbol{\Sigma}_{\mathbb{S},\mathbb{S}}^{-1} \boldsymbol{\Sigma}_{\mathbb{S},\mathbb{S}^{\complement}}.
\end{aligned}$$

The remaining question is how to choose the intervention logits $\boldsymbol{\eta}'_{\mathbb{S}}$. In the standard CBM setting, Koh et al. (2020) set each intervention logit η'_i to the empirical 95th percentile of the training logits when the corrected concept value is $c_i = 1$, and to the empirical 5th percentile when $c_i = 0$. Although this percentile-based strategy can be applied to SCBM, it can be suboptimal when interventions are propagated through the learned covariance structure (Vandenhirtz et al., 2024).

First, if the original predicted mean μ_i is already more extreme than the selected percentile, replacing η_i with the fixed percentile can move the intervention logit in the wrong direction. This incorrect displacement is then propagated to the non-intervened logits through the conditional update of $\bar{\boldsymbol{\mu}}_{\mathbb{S}^{\complement}}$. As a result, the updated non-intervened logits may be shifted in an unintended direction. Second, choosing intervention logits too far from $\boldsymbol{\mu}_{\mathbb{S}}$ can make the conditional mean shift $\boldsymbol{\Sigma}_{\mathbb{S}^{\complement},\mathbb{S}} \boldsymbol{\Sigma}_{\mathbb{S},\mathbb{S}}^{-1} (\boldsymbol{\eta}'_{\mathbb{S}} - \boldsymbol{\mu}_{\mathbb{S}})$ dominate the original mean prediction for the non-intervened logits.

Vandenhirtz et al. (2024) therefore require the intervention logits to satisfy two conditions. First, each logit must move in the direction of the corrected concept value:

$$\eta_i - \mu_i \geq 0 \quad \text{if } c'_i = 1, \qquad \eta_i - \mu_i \leq 0 \quad \text{if } c'_i = 0.$$

Second, the intervention logits should remain plausible under the predicted Gaussian distribution. Since we model $\boldsymbol{\eta}$ as a multivariate Gaussian, the marginal distribution of $\boldsymbol{\eta}_{\mathbb{S}}$ for any subset $\mathbb{S}$ is also Gaussian:

$$\boldsymbol{\eta}_{\mathbb{S}} \sim \mathcal{N}(\boldsymbol{\mu}_{\mathbb{S}}, \boldsymbol{\Sigma}_{\mathbb{S},\mathbb{S}}).$$

By the property of multivariate Gaussian distributions, the squared Mahalanobis distance

$$d_M^2(\boldsymbol{\eta}_{\mathbb{S}}, \boldsymbol{\mu}_{\mathbb{S}}) = (\boldsymbol{\eta}_{\mathbb{S}} - \boldsymbol{\mu}_{\mathbb{S}})^\top \boldsymbol{\Sigma}_{\mathbb{S},\mathbb{S}}^{-1} (\boldsymbol{\eta}_{\mathbb{S}} - \boldsymbol{\mu}_{\mathbb{S}})$$

follows a Chi-squared distribution with $|\mathbb{S}|$ degrees of freedom. This gives the following Mahalanobis-distance constraint on the intervention logits:

$$d_M^2(\boldsymbol{\eta}_{\mathbb{S}}, \boldsymbol{\mu}_{\mathbb{S}}) \leq \chi^2_{|\mathbb{S}|,1-\alpha},$$

where $\chi^2_{|\mathbb{S}|,1-\alpha}$ is the $(1-\alpha)$-quantile of the Chi-squared distribution with $|\mathbb{S}|$ degrees of freedom, and we use $\alpha = 0.01$ in our experiments. Combining these conditions, Vandenhirtz et al. (2024) formulate the selection of intervention logits as the following constrained optimization problem:

$$\boldsymbol{\eta}'_{\mathbb{S}} = \arg\max_{\boldsymbol{\eta}_{\mathbb{S}}} \log p(\boldsymbol{c}'_{\mathbb{S}} \mid \boldsymbol{\eta}_{\mathbb{S}})$$

$$\text{s.t.} \quad \begin{cases} \eta_i \geq \mu_i, & \text{if } c'_i = 1 \\ \eta_i \leq \mu_i, & \text{if } c'_i = 0 \end{cases} \quad \forall i \in \mathbb{S},$$

$$\text{and} \quad (\boldsymbol{\eta}_{\mathbb{S}} - \boldsymbol{\mu}_{\mathbb{S}})^\top \boldsymbol{\Sigma}_{\mathbb{S},\mathbb{S}}^{-1} (\boldsymbol{\eta}_{\mathbb{S}} - \boldsymbol{\mu}_{\mathbb{S}}) \leq \chi^2_{|\mathbb{S}|,1-\alpha}.$$

When predicting the target label $\hat{y}'$ under interventions, the intervention logits $\boldsymbol{\eta}'_{\mathbb{S}}$ are computed via the constrained optimization problem. The non-intervened logits $\boldsymbol{\eta}_{\mathbb{S}^\complement}$ are subsequently sampled from the resulting conditional Gaussian distribution. Finally, the non-intervened concepts sampled from these updated logits are combined with the ground-truth binary values of the intervened concepts, and this joint concept vector is used to predict the final target $\hat{y}'$.

4 Experimental Setup

4.1 Datasets and Evaluation

Synthetic Dataset The synthetic dataset follows the correlated-concept construction of Vandenhirtz et al. (2024). It contains $N = 50{,}000$ samples with $C = 100$ binary concepts and $p = 1{,}500$ observed input features, split into train, validation, and test sets with a 60%/20%/20% ratio. The dataset is designed as a controlled benchmark with correlated concepts, allowing us to test whether modeling concept dependencies improves predictive and intervention performance. The data generation procedure is summarized in Appendix B.1.

Natural Image Datasets For the natural image experiments, we use the Caltech-UCSD Birds-200-2011 dataset (CUB-200-2011) (Wah et al., 2011) and CIFAR-10 (Krizhevsky et al., 2009). CUB-200-2011 contains 11,788 images from 200 bird species. The image classification task uses the 112 binary bird attributes selected in the original CBM work (Koh et al., 2020) as concepts and bird species as target labels. For CIFAR-10, following the setup of Vandenhirtz et al. (2024), we use a CLIP-based concept-labeling pipeline to reduce the need for manual concept annotations. The concept vocabulary consists of 143 concepts generated with GPT-3 in prior work on label-free CBMs (Brown et al., 2020; Oikarinen et al., 2023). Binary concept labels are generated before training by comparing CLIP (Radford et al., 2021) similarities between each image and paired positive and negative text prompts, such as “machine” and “not machine”.

Evaluation To compare models, we evaluate predictive performance and concept-probability calibration. Predictive performance is measured by concept accuracy and target accuracy on the test set. Calibration is measured using the Brier score (Glenn, 1950) and binary Expected Calibration Error (ECE) (Naeini et al., 2015; Kumar et al., 2019). For both calibration metrics, we treat each sample-concept pair as a Bernoulli probability prediction and average over all sample-concept pairs. The full definitions of the Brier score and ECE used in our experiments are provided in Appendix B.2.

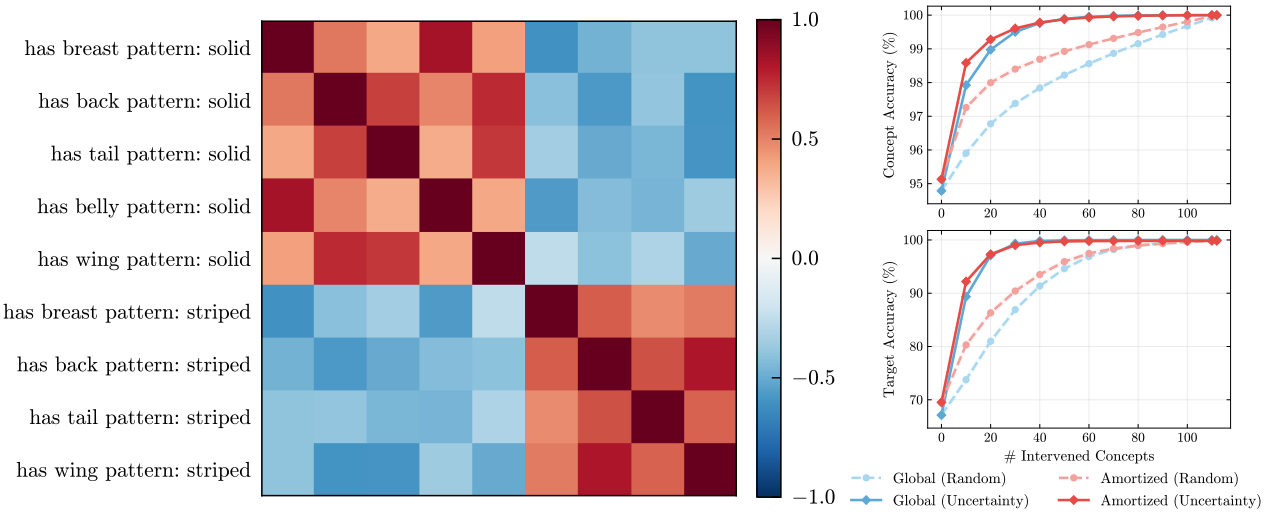

(a) Learned global covariance matrix example.

(b) Intervention performance.

Figure 2: CUB analysis of learned concept dependencies and uncertainty-guided interventions. **(a)** A subset of the global covariance matrix learned by Global SCBM, illustrating dataset-level dependency structure among selected concepts. **(b)** Intervention performance of SCBMs measured in concept and target accuracy (%) on CUB for random and uncertainty-based policy.

4.2 Baselines

We compare SCBM with Hard CBM, autoregressive CBM (Havasi et al., 2022), and CEM (Espinosa Zarlenga et al., 2022). These baselines cover three relevant alternatives to SCBM: a hard binary bottleneck without dependency-aware updates, an order-dependent approach to modeling concept correlations, and an embedding-based concept bottleneck. The model comprises a backbone for concept prediction and a linear target head that maps concept representations to target predictions. Detailed hyperparameters and model architectures are provided in Appendix C.

For SCBM, we evaluate two covariance parameterizations considered by Vandenhirtz et al. (2024): an amortized variant, where the covariance matrix $\boldsymbol{\Sigma}(\boldsymbol{x})$ is predicted for each input, and a global variant, where a single covariance matrix $\boldsymbol{\Sigma}$ is learned for the entire dataset. The global variant may be preferable in settings where a fixed concept dependency structure is a strong prior.

5 Main Results

5.1 Test Performance

In Table 1, we report predictive performance and calibration metrics on the test set before intervention. In terms of concept and target accuracy, SCBM performs competitively with the baselines, and no model consistently dominates across all datasets. This suggests that modeling concept dependencies does not come at a clear cost in predictive performance.

We also observe that the amortized SCBM variant consistently outperforms the global covariance variant across the three datasets, suggesting that the additional flexibility of instance-wise covariance prediction may be useful in these settings. In contrast, the global covariance variant provides a single dataset-level dependency structure that is easier to inspect. For example, the selected body-pattern attributes in Figure 2a show interpretable correlation patterns: striped-pattern attributes are positively correlated with each other, solid-pattern attributes are positively correlated with each other, and striped patterns are negatively correlated with solid patterns.

Table 1: Test-set performance across ten random seeds before intervention, reported as mean ± sample standard deviation. Concept accuracy, target accuracy, Brier score, and ECE are reported as percentages. **Bold** and underlined mean values indicate the best and second-best results for each metric and dataset, respectively; higher is better for accuracies, and lower is better for Brier score and ECE.

Dataset	Model	Concept Accuracy	Target Accuracy	Brier	ECE
Synthetic	Hard CBM	69.33 ± 0.07	66.76 ± 0.24	20.02 ± 0.04	5.89 ± 0.14
	CEM	69.37 ± 0.08	66.79 ± 0.37	20.08 ± 0.04	6.16 ± 0.09
	Autoregressive CBM	$\mathbf{70.66} \pm 0.03$	67.28 ± 0.15	$\mathbf{18.97} \pm 0.02$	2.34 ± 0.09
	Global SCBM	70.50 ± 0.04	$\underline{67.43} \pm 0.20$	19.04 ± 0.02	$\underline{2.31} \pm 0.07$
	Amortized SCBM	$\underline{70.53} \pm 0.05$	$\mathbf{67.47} \pm 0.13$	$\underline{19.01} \pm 0.02$	$\mathbf{2.11} \pm 0.07$
CUB	Hard CBM	94.83 ± 0.07	67.11 ± 0.68	4.02 ± 0.08	2.48 ± 0.13
	CEM	94.94 ± 0.09	68.79 ± 0.66	4.17 ± 0.08	3.34 ± 0.10
	Autoregressive CBM	$\mathbf{95.24} \pm 0.09$	$\underline{68.83} \pm 0.58$	$\underline{3.84} \pm 0.07$	2.82 ± 0.10
	Global SCBM	94.79 ± 0.11	67.10 ± 0.76	4.01 ± 0.09	$\underline{2.41} \pm 0.09$
	Amortized SCBM	$\underline{95.13} \pm 0.10$	$\mathbf{69.44} \pm 0.59$	$\mathbf{3.70} \pm 0.08$	$\mathbf{1.90} \pm 0.09$
CIFAR-10	Hard CBM	85.48 ± 0.07	69.72 ± 0.20	10.50 ± 0.06	5.29 ± 0.12
	CEM	85.23 ± 0.17	$\mathbf{72.17} \pm 0.61$	10.84 ± 0.22	6.46 ± 0.55
	Autoregressive CBM	85.57 ± 0.10	69.56 ± 0.53	10.40 ± 0.12	5.23 ± 0.35
	Global SCBM	$\underline{85.87} \pm 0.03$	70.89 ± 0.37	$\underline{9.98} \pm 0.02$	$\underline{3.15} \pm 0.07$
	Amortized SCBM	$\mathbf{86.08} \pm 0.07$	$\underline{71.97} \pm 0.26$	$\mathbf{9.78} \pm 0.05$	$\mathbf{1.96} \pm 0.22$

An interesting pattern can be observed in the CIFAR-10 dataset. Although CEM has the lowest concept accuracy among the compared models, it achieves the highest target accuracy. This pattern is consistent with the possibility that the high-dimensional concept embeddings carry task-relevant information beyond the scalar concept predictions. This suggests the expressiveness-interpretability trade-off in concept-based models: richer concept representations can improve target performance, but they may weaken the extent to which the target prediction can be understood solely through concept probabilities.

The calibration results further support the benefit of SCBM's explicit distributional parameterization of concepts. In Table 1, amortized SCBM achieves the best ECE across all three datasets and the best or second-best Brier score, suggesting more reliable concept-probability estimates. Reliable concept uncertainty estimates are particularly relevant for intervention. At each intervention step, the uncertainty-based policy selects the concept with the highest predictive uncertainty, aiming to improve intervention efficiency by correcting uncertain concepts earlier. Here, uncertainty is measured by the proximity of the predicted concept probability to 0.5; that is, the concept with the smallest $|\hat{p} - 0.5|$ is selected for intervention. We compare random and uncertainty-based intervention policies for SCBM on CUB. As shown in Figure 2b, the substantial gap between the two policies indicates that SCBM's predicted concept probabilities carry meaningful uncertainty information for guiding interventions.

5.2 Intervention

Figure 3 shows intervention performance across datasets under the uncertainty-based intervention policy described above. The curves report concept and target accuracy after intervening on an increasing number of concepts. For concept prediction, SCBM variants generally show steeper improvement than the baselines, indicating that each manual correction improves not only the intervened concept but also related non-intervened concepts. This behavior is consistent with the dependency-aware intervention mechanism introduced in Section 3.2, which propagates intervention information to correlated concepts through the learned dependency structure. Similarly, the target accuracy curves show that the improved concept predictions also translate to improvements in target prediction. Notably, in the most practical scenario with a small number of interventions, SCBM consistently outperforms the baselines in both concept and target accuracy, indicating the value of modeling concept dependencies for efficient and effective interventions.

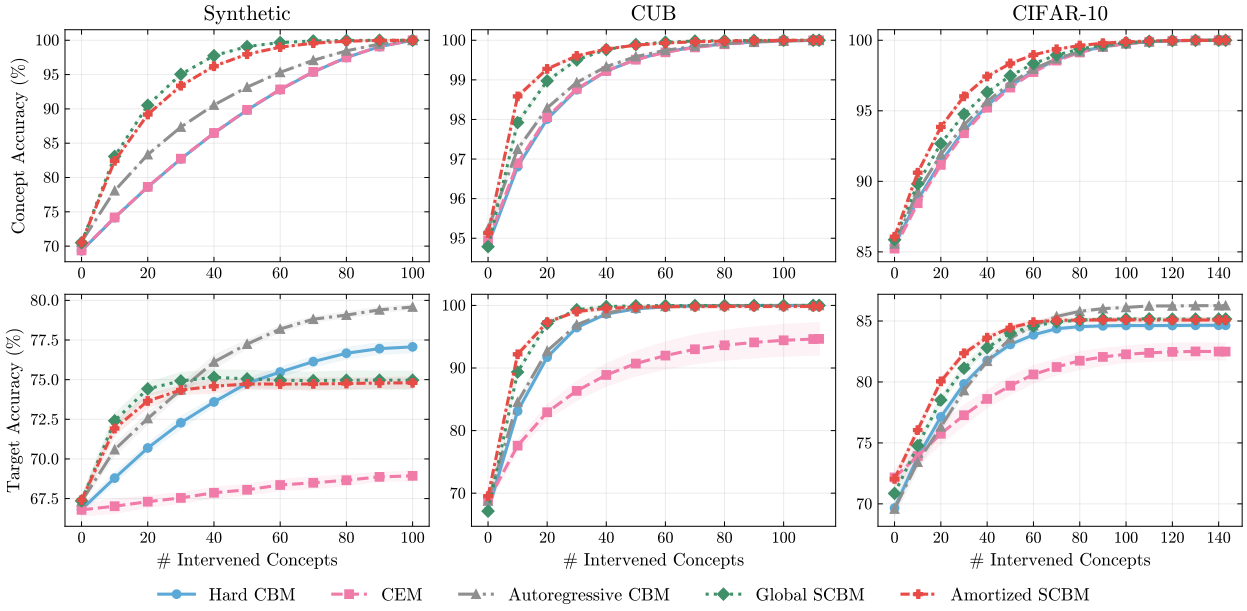

Figure 3: Intervention performance across datasets and models. The x-axis shows the number of intervened concepts, and the y-axis shows accuracy after intervention. Curves are averaged over ten random seeds, and shaded areas indicate ± one sample standard deviation.

The two SCBM variants behave differently across datasets. On the natural image datasets, amortized SCBM generally outperforms global SCBM, consistent with the test-set results in Table 1. This suggests that input-dependent covariance prediction can be useful when concept dependencies vary across instances. On the synthetic dataset, global SCBM performs slightly better, which is consistent with the data generation process having a fixed covariance structure shared across samples.

Autoregressive CBM also models concept dependencies and therefore improves over Hard CBM in intervention as expected. However, its advantage over SCBM appears mainly at larger intervention budgets in the target accuracy curves. This setting is less aligned with the intended use case of concept interventions, where the goal is to obtain large performance gains from only a small number of manual corrections. The better performance of autoregressive CBM at larger intervention budgets may partly benefits from the independent training procedure used for autoregressive CBMs, where the target predictor is trained using ground-truth concept labels rather than predicted concepts. Finally, CEM shows weaker target intervention performance in our experiments, which may be explained by the omission of the intervention-specific optimization from the original CEM framework (Espinosa Zarlenga et al., 2022), as Vandenhirtz et al. (2024) exclude it to maintain a fair comparison across models.

6 Practical Reproduction Findings

Beyond reproducing the empirical results, we study the practical cost of reproducing SCBM. Vandenhirtz et al. (2024) report that reproducing the full set of experiments with the original implementation requires approximately 1,200 GPU hours on GeForce RTX 2080 hardware. To make the reproduction feasible within our compute budget, we ran our experiments on a GeForce RTX 4090. However, our initial profiling showed that the original implementation remained slow even on stronger hardware, with low and unstable GPU utilization. Through iterative profiling and optimization, we identified overhead from several parts of the pipeline, including CPU-bound data loading, unnecessary metric computation during training, model-forward overhead from naive for loops, and repeated intervention-time CPU–GPU data transfer.

We addressed these bottlenecks through four types of optimizations. First, we optimized the data pipeline by moving suitable transformations to batched GPU execution. Second, we vectorized model execution while

Table 2: Timing comparison between the legacy and optimized implementations on CIFAR-10.

Dataset	Model	Stage	Legacy (s)	Optimized (s)	Speedup
CIFAR-10	Autoregressive CBM	pretrain	188.2	8.7	21.6×
		concept	198.4	11.4	17.4×
		target	111.8	3.6	31.1×
		intervention	1264.6	86.1	14.7×
	CEM	joint	263.3	12.6	20.9×
		intervention	185.5	74.5	2.5×
	Hard CBM	joint	112.8	14.0	8.1×
		intervention	193.3	73.3	2.6×
	Amortized SCBM	joint	120.2	29.3	4.1×
		intervention	278.4	104.8	2.7×
	Global SCBM	joint	124.6	27.5	4.5×
		intervention	504.8	104.2	4.8×

preserving the original computation, including batched concept-embedding computation for CEM, parallel teacher-forced concept prediction for autoregressive CBM, and batched Monte Carlo samples prediction for all models requiring Monte Carlo sampling. Third, we changed intervention evaluation from a step-first order to a batch-first order, so that intermediate intervention states remain on the GPU across intervention steps. Fourth, for SCBM dependency-aware interventions, we replaced the per-sample CPU-based SLSQP solver (Kraft, 1988; Virtanen et al., 2020) with a batched Frank-Wolfe solver (Frank & Wolfe, 1956) implemented in PyTorch, which produces numerically close solutions while substantially reducing solver runtime. Further implementation details and validation results are provided in Appendix D.

These optimizations substantially reduce the practical cost of reproduction. On a single GeForce RTX 4090, we completed the reproduction in approximately 62 wall-clock hours. In Table 2, we compare the runtime on the CIFAR-10 dataset between the legacy and optimized implementations using a single GeForce RTX 4090, ensuring that the reported speedups strictly isolate the effect of our optimizations. The benchmark is reported by model and stage. For the autoregressive CBM, *pretrain* denotes pretraining of the autoregressive concept predictors, *concept* denotes training of the encoder and concept predictors, and *target* denotes training of the target head. For the other models, *joint* denotes joint training of the encoder, concept predictor, and target head. The *intervention* stage denotes intervention evaluation. Training-stage runtimes are measured over five training epochs using the hyperparameters in Table 3. Intervention runtimes include initialization and intervention evaluation over two batches of 64 samples. The benchmark results of other datasets are available in Appendix D.6.

More importantly, the optimized implementation changes the relative runtime behavior of the compared models. Vandenhirtz et al. (2024) report that SCBM is much more efficient than autoregressive CBM during evaluation, and has comparable training time with other baselines. However, the optimized benchmark in Table 2 shows a different runtime ordering during intervention evaluation. With proper implementation, autoregressive CBM can achieve intervention-evaluation runtimes comparable to SCBM, and SCBM's training time is often longer than other baselines due to the additional computational overhead of learning and sampling from the joint Gaussian distribution. This suggests that runtime comparisons should be interpreted as properties of a method–implementation pair rather than of the method alone. Therefore, our reproduction supports SCBM's main methodological value in dependency-aware intervention, while suggesting that claims about computational efficiency are implementation-sensitive.

7 Conclusion

In this reproduction study, we reproduced the key experiments of the SCBM framework proposed by Vandenhirtz et al. (2024) on a synthetic dataset and two natural image datasets. Overall, our results are broadly consistent with the original paper and support the reproducibility of its main empirical claims. In particular,

SCBM models concept dependencies without a clear degradation in predictive performance before intervention, and achieves stronger concept-probability calibration than the compared baselines. The global SCBM variant also provides a valuable tool for inspecting dataset-level concept relationships.

Our intervention experiments further support the main motivation of SCBM: modeling concept dependencies can make concept interventions more efficient. By propagating the effect of a corrected concept to correlated non-intervened concepts, SCBM improves concept and target accuracy with fewer manual interventions. We also find that SCBM benefits from uncertainty-based intervention policies, which prioritize concepts whose predicted probabilities are closest to 0.5, suggesting that SCBM's concept-probability estimates carry useful uncertainty signals for selecting interventions and reducing the need for users to manually search through the full concept set.

Beyond empirical reproduction, we examined the practical cost of reproducing SCBM. Starting from the official implementation, we identified several implementation bottlenecks and refactored the experimental pipeline to reduce avoidable overhead while preserving the intended model definitions and evaluation protocol. This substantially reduced the practical reproduction cost on modern hardware and made it possible to complete the experiments in approximately 62 wall-clock hours on a single GeForce RTX 4090.

We also revisited the computational-efficiency interpretation of SCBM. After optimization, the relative runtime behavior of SCBM and the baselines differs from that reported with the original implementation, indicating that runtime comparisons are sensitive to implementation choices. We therefore suggest that the practical value of SCBM should be framed less around raw computational efficiency and more around its ability to perform dependency-aware interventions without relying on the fixed concept ordering imposed by autoregressive CBMs, which may not correspond to a natural semantic or causal structure in the data.

References

Tom Brown, Benjamin Mann, Nick Ryder, Melanie Subbiah, Jared D Kaplan, Prafulla Dhariwal, Arvind Neelakantan, Pranav Shyam, Girish Sastry, Amanda Askell, et al. Language models are few-shot learners. *Advances in Neural Information Processing Systems*, 33:1877–1901, 2020.

Mateo Espinosa Zarlenga, Pietro Barbiero, Gabriele Ciravegna, Giuseppe Marra, Francesco Giannini, Michelangelo Diligenti, Zohreh Shams, Frederic Precioso, Stefano Melacci, Adrian Weller, et al. Concept embedding models: Beyond the accuracy-explainability trade-off. *Advances in Neural Information Processing Systems*, 35:21400–21413, 2022.

Marguerite Frank and Philip Wolfe. An algorithm for quadratic programming. *Naval research logistics quarterly*, 3(1-2):95–110, 1956.

Jerome Friedman, Trevor Hastie, and Robert Tibshirani. Sparse inverse covariance estimation with the graphical lasso. *Biostatistics*, 9(3):432–441, 2008.

W. Brier Glenn. Verification of forecasts expressed in terms of probability. *Monthly weather review*, 78(1): 1–3, 1950.

Marton Havasi, Sonali Parbhoo, and Finale Doshi-Velez. Addressing leakage in concept bottleneck models. *Advances in Neural Information Processing Systems*, 35:23386–23397, 2022.

Kaiming He, Xiangyu Zhang, Shaoqing Ren, and Jian Sun. Deep residual learning for image recognition. In *Proceedings of the IEEE conference on computer vision and pattern recognition*, pp. 770–778, 2016.

Eric Jang, Shixiang Gu, and Ben Poole. Categorical reparameterization with gumbel-softmax. In *International Conference on Learning Representations*, 2017.

Diederik P Kingma and Jimmy Ba. Adam: A method for stochastic optimization. *arXiv preprint arXiv:1412.6980*, 2014.

Pang Wei Koh, Thao Nguyen, Yew Siang Tang, Stephen Mussmann, Emma Pierson, Been Kim, and Percy Liang. Concept bottleneck models. In *International conference on machine learning*, pp. 5338–5348. PMLR, 2020.

Dieter Kraft. A software package for sequential quadratic programming. *Forschungsbericht- Deutsche Forschungs- und Versuchsanstalt fur Luft- und Raumfahrt*, 1988.

Alex Krizhevsky, Geoffrey Hinton, et al. Learning multiple layers of features from tiny images. 2009.

Ananya Kumar, Percy S Liang, and Tengyu Ma. Verified uncertainty calibration. *Advances in Neural Information Processing Systems*, 32, 2019.

Chris J. Maddison, Andriy Mnih, and Yee Whye Teh. The concrete distribution: A continuous relaxation of discrete random variables. In *International Conference on Learning Representations*, 2017.

Anita Mahinpei, Justin Clark, Isaac Lage, Finale Doshi-Velez, and Weiwei Pan. Promises and pitfalls of black-box concept learning models. *arXiv preprint arXiv:2106.13314*, 2021.

TorchVision maintainers and contributors. Torchvision: Pytorch's computer vision library. `https://github.com/pytorch/vision`, 2016.

Andrei Margeloiu, Matthew Ashman, Umang Bhatt, Yanzhi Chen, Mateja Jamnik, and Adrian Weller. Do concept bottleneck models learn as intended? *arXiv preprint arXiv:2105.04289*, 2021.

Mahdi Pakdaman Naeini, Gregory Cooper, and Milos Hauskrecht. Obtaining well calibrated probabilities using bayesian binning. In *Proceedings of the AAAI conference on artificial intelligence*, volume 29, 2015.

Tuomas Oikarinen, Subhro Das, Lam M Nguyen, and Tsui-Wei Weng. Label-free concept bottleneck models. In *International Conference on Learning Representations*, 2023.

Alec Radford, Jong Wook Kim, Chris Hallacy, Aditya Ramesh, Gabriel Goh, Sandhini Agarwal, Girish Sastry, Amanda Askell, Pamela Mishkin, Jack Clark, et al. Learning transferable visual models from natural language supervision. In *International conference on machine learning*, pp. 8748–8763. PmLR, 2021.

Ivaxi Sheth, Aamer Abdul Rahman, Laya Rafiee Sevyeri, Mohammad Havaei, and Samira Ebrahimi Kahou. Learning from uncertain concepts via test time interventions. In *Workshop on trustworthy and socially responsible machine learning, neurips 2022*, 2022.

Sungbin Shin, Yohan Jo, Sungsoo Ahn, and Namhoon Lee. A closer look at the intervention procedure of concept bottleneck models. In *International conference on machine learning*, pp. 31504–31520. PMLR, 2023.

Moritz Vandenhirtz, Sonia Laguna, Ričards Marcinkevičs, and Julia E Vogt. Stochastic concept bottleneck models. *Advances in Neural Information Processing Systems*, 37:51787–51810, 2024.

Pauli Virtanen, Ralf Gommers, Travis E Oliphant, Matt Haberland, Tyler Reddy, David Cournapeau, Evgeni Burovski, Pearu Peterson, Warren Weckesser, Jonathan Bright, et al. Scipy 1.0: fundamental algorithms for scientific computing in python. *Nature methods*, 17(3):261–272, 2020.

Catherine Wah, Steve Branson, Peter Welinder, Pietro Perona, and Serge Belongie. The caltech-ucsd birds-200-2011 dataset. (CNS-TR-2011-001), 2011.

A Monte Carlo Estimators for Concept Loss

To learn the concept distribution, SCBM minimizes the negative marginal log-likelihood of the observed concept labels. For a single data point $(\boldsymbol{x}, \boldsymbol{c})$, the concept loss is

$$\mathcal{L}_c = -\log p(\boldsymbol{c} \mid \boldsymbol{x}) = -\log \int p(\boldsymbol{c} \mid \boldsymbol{\eta}) p_\phi(\boldsymbol{\eta} \mid \boldsymbol{x}) d\boldsymbol{\eta},$$

where $p_\phi(\boldsymbol{\eta} \mid \boldsymbol{x})$ denotes the multivariate Gaussian $\mathcal{N}\big(\boldsymbol{\mu}(\boldsymbol{x}), \boldsymbol{\Sigma}(\boldsymbol{x})\big)$ parameterized by the neural network encoder with parameters ϕ. This integral is intractable due to the sigmoid-transform applied to the concept

logits in the Bernoulli likelihood. SCBM therefore approximates the marginal likelihood using M Monte Carlo samples: $\boldsymbol{\eta}^{(m)} \sim \mathcal{N}(\boldsymbol{\mu}(\boldsymbol{x}), \boldsymbol{\Sigma}(\boldsymbol{x}))$:

$$\mathcal{L}_c \approx -\log\left(\frac{1}{M}\sum_{m=1}^{M} p(\boldsymbol{c} \mid \boldsymbol{\eta}^{(m)})\right).$$

To enable end-to-end backpropagation through this sampling process, SCBMs employ the reparameterization trick:

$$\boldsymbol{\eta}^{(m)} = \boldsymbol{\mu}(\boldsymbol{x}) + \boldsymbol{L}(\boldsymbol{x})\boldsymbol{\epsilon}^{(m)}, \qquad \boldsymbol{\epsilon}^{(m)} \sim \mathcal{N}(\boldsymbol{0}, \boldsymbol{I}),$$

where $\boldsymbol{L}(\boldsymbol{x})$ is the Cholesky factor of $\boldsymbol{\Sigma}(\boldsymbol{x})$, so that $\boldsymbol{L}(\boldsymbol{x})\boldsymbol{L}(\boldsymbol{x})^T = \boldsymbol{\Sigma}(\boldsymbol{x})$.

Using the conditional independence assumption, the concept loss can be rewritten in log-space directly in terms of the Binary Cross-Entropy (BCE) loss for each concept:

$$\begin{aligned}
\mathcal{L}_c &\approx -\log\left(\frac{1}{M}\sum_{m=1}^{M} p(\boldsymbol{c} \mid \boldsymbol{\eta}^{(m)})\right) \\
&= -\log\left(\frac{1}{M}\sum_{m=1}^{M} \exp\sum_{i=1}^{C} \log p(c_i \mid \eta_i^{(m)})\right) \\
&= -\log\left(\frac{1}{M}\sum_{m=1}^{M} \exp\left[-\sum_{i=1}^{C} \mathrm{BCE}\big(c_i,\, \sigma(\eta_i^{(m)})\big)\right]\right).
\end{aligned}$$

This factorization allows all concepts to be sampled in parallel for a given logit vector, enabling efficient joint training of both the concept and target predictors. In contrast, in the autoregressive CBM (Havasi et al., 2022), concept sampling is sequential and the target predictor is trained independently for efficiency.

B Dataset and Evaluation Details

B.1 Synthetic Dataset Generation

The synthetic data generation procedure used by Vandenhirtz et al. (2024) is summarized as follows. Let $\{(\boldsymbol{x}_n, \boldsymbol{c}_n, y_n)\}_{n=1}^{N}$ denote the dataset, where $\boldsymbol{x}_n \in \mathbb{R}^p$ is the observed input feature vector, $\boldsymbol{c}_n \in \{0,1\}^C$ is the binary concept vector, and y_n is the target label. We use $N = 50{,}000$, $p = 1{,}500$, and $C = 100$, with a 60%/20%/20% train/validation/test split. Concept dependencies are generated through correlated latent logits. The concept-logit covariance matrix is sampled in low-rank-plus-diagonal form as

$$\boldsymbol{\Sigma} = \boldsymbol{W}\boldsymbol{W}^T + \boldsymbol{D},$$

where $\boldsymbol{W} \in \mathbb{R}^{C\times 10}$ has entries sampled from $\mathcal{N}(0,1)$ and $\boldsymbol{D} = \mathrm{diag}(\delta_1, \ldots, \delta_C)$ with $\delta_i \sim \mathcal{U}[0,1]$. For each sample, latent logits are drawn as

$$\boldsymbol{\eta}_n \sim \mathcal{N}(\boldsymbol{0}, \boldsymbol{\Sigma}),$$

and binary concepts are obtained by thresholding the logits:

$$c_{n,i} = \boldsymbol{1}\{\eta_{n,i} \geq 0\}.$$

Observed input features are generated by applying a randomly initialized MLP $f : \mathbb{R}^C \to \mathbb{R}^p$ with two hidden layers of width d_h and ReLU activations to the latent logits, followed by additive Gaussian noise:

$$\tilde{\boldsymbol{x}}_n = f(\boldsymbol{\eta}_n) + \boldsymbol{\epsilon}_n, \qquad \boldsymbol{\epsilon}_n \sim \mathcal{N}(\boldsymbol{0}, \delta \boldsymbol{I}_p).$$

Following Vandenhirtz et al. (2024), the MLP outputs are normalized across the full dataset before adding Gaussian noise, and the noisy features are normalized again across the full dataset to obtain the final observed features $\boldsymbol{x}_n$. The original codebase uses $d_h = 5$ and $\delta = 1$. However, we found that this setting makes the

dataset too noisy for all models to learn meaningful signals, so we set $d_h = 10$ to preserve more information in $\boldsymbol{x}$ and $\delta = 0.5$ to reduce the noise level.

Finally, target labels are generated by applying a randomly initialized linear map $g : \mathbb{R}^C \to \mathbb{R}$ to the binary concept vectors. Let $s_n = g(\boldsymbol{c}_n)$ and let s_{med} denote the median of $\{s_n\}_{n=1}^N$. The target label is defined as

$$y_n = \mathbf{1}\{s_n \geq s_{\text{med}}\},$$

which yields a balanced binary classification task.

B.2 Calibration Metrics

Let N denote the number of evaluation samples and C the number of concepts. Let $c_{n,j} \in \{0, 1\}$ denote the ground-truth value of concept j for sample n, and let $\hat{p}_{n,j}$ denote the predicted probability that this concept is present. We evaluate calibration by treating each sample-concept pair (n, j) as a Bernoulli probability prediction.

The Brier score measures the mean squared error between predicted concept probabilities and binary concept labels:

$$\text{Brier} = \frac{1}{NC} \sum_{n=1}^{N} \sum_{j=1}^{C} (\hat{p}_{n,j} - c_{n,j})^2.$$

ECE measures the same probabilities from a binned calibration perspective. We divide $[0, 1]$ into $K = 10$ uniformly spaced intervals $\{\mathcal{I}_k\}_{k=1}^K$ and define

$$\mathcal{B}_k = \{(n, j) : \hat{p}_{n,j} \in \mathcal{I}_k\}.$$

For each non-empty bin, we compute the empirical frequency of positive concept labels, denoted by freq_k, and the average predicted probability of concept presence, denoted by conf_k:

$$\text{freq}_k = \frac{1}{|\mathcal{B}_k|} \sum_{(n,j) \in \mathcal{B}_k} c_{n,j}, \qquad \text{conf}_k = \frac{1}{|\mathcal{B}_k|} \sum_{(n,j) \in \mathcal{B}_k} \hat{p}_{n,j}.$$

The ECE is then computed as:

$$\text{ECE} = \sum_{k=1}^{K} \frac{|\mathcal{B}_k|}{NC} \left| \text{freq}_k - \text{conf}_k \right|.$$

C Model Configurations and Hyperparameters

We summarize the model configurations and training hyperparameters used in our experiments. Each experiment is run over ten random seeds. All models are trained with the Adam optimizer (Kingma & Ba, 2014) and weight decay 10^{-4}. To ensure a fair comparison between different models, all models use the same dataset-specific encoder architecture and a linear target head that maps the model's concept representation to target predictions. The dataset-specific training settings and encoder choices are summarized in Table 3.

Table 3: Dataset-specific training settings and encoder architectures.

Dataset	Epochs	Batch size	Learning rate	Encoder
Synthetic	150	256	10^{-4}	Three-block fully connected network
CUB	300	64	10^{-4}	ResNet18 (He et al., 2016)
CIFAR-10	300	256	2×10^{-4}	Small CNN

The synthetic encoder is a three-block fully connected network, where each block consists of a linear layer, batch normalization, ReLU activation, and dropout. The CIFAR-10 encoder is a small CNN with two

convolutional layers, ReLU activations, and max pooling, followed by dropout and a linear layer. The CUB experiments use a ResNet18 encoder (He et al., 2016).

The autoregressive CBM uses an additional 50-epoch pretraining stage for the concept predictors to obtain a stable initialization. Sampling-based methods use $M = 100$ Monte Carlo samples. Amortized SCBM uses $\lambda_y = 1.0$ and $\lambda_{\text{reg}} = 1.0$, while Global SCBM uses $\lambda_y = 1.0$ and $\lambda_{\text{reg}} = 0.0$.

D Refactoring and Optimization Details

In this section, we summarize the main optimization categories and report benchmarks comparing the original and optimized implementations on our hardware, isolating the contribution of the implementation changes from hardware differences.

D.1 General Refactoring

The original implementation tightly couples model-specific training logic, stage control, metric computation, and model-forward logic. As a first step, we refactored the training pipeline into a more modular structure. We implemented a staged experiment runner that makes model-specific training stages explicit, including the pretraining, concept-predictor training and target-head training of autoregressive CBM, and joint training for the other models. We also introduced model adapters to expose a consistent interface across models, allowing the same runner to apply consistent freezing policies, optimizer construction, and metric computation.

We also reorganized the model-forward logic. The legacy implementation keeps multiple baseline variants inside a single model wrapper and dispatches behavior through many if-else statements depending on the configuration. To preserve compatibility with the original interface, we did not fully split the implementation into separate model classes. Instead, we factored model-specific logic into separate methods while retaining the outer wrapper for input dispatch and output collection. This compromise improved readability and reduced duplicated conditional logic while keeping the refactoring scope manageable.

Finally, we simplified the metrics computed during training. We retained lightweight concept and target accuracy for training-time monitoring, while reserving more expensive calibration metrics, such as Brier score and ECE, for validation and test evaluation. This reduced avoidable CPU overhead during training without changing the evaluation protocol.

D.2 Data Pipeline Optimizations

Profiling showed that the natural-image experiments were often limited by CPU-side data processing. In particular, repeated disk reads, PIL image decoding, and image transformations such as resizing, cropping, and data augmentation caused unstable GPU utilization. We therefore optimized the data pipeline to reduce repeated CPU work while preserving the preprocessing semantics of the original implementation.

For CIFAR-10, the full dataset is small enough to fit in memory, eliminating disk reads as a bottleneck. The remaining CPU overhead mainly comes from repeated CPU-side transform applied on every iteration. We address this by adopting the `torchvision` (maintainers & contributors, 2016) v2 transform API, which allows batch-level transforms to be executed on the GPU, leaving only minimal logic on the CPU side.

For CUB, a caching strategy implemented by the community[1] eliminates the dominant overhead from repeated disk reads and PIL decoding. For the remaining transforms, because CUB images vary in original resolution, each sample must first be individually loaded and cropped to a uniform size via `RandomResizedCrop` before batching is possible. This per-sample operation depends on the original image geometry and must remain on the CPU. Other transforms such as augmentation and normalization are moved to the GPU. As a result, CUB remains more CPU-bound than the synthetic and CIFAR-10 datasets, but the optimized pipeline still reduces avoidable data-loading overhead.

[1] https://medium.com/@maxwbuckley/making-stochastic-concept-bottleneck-models-go-brrrr-with-birds-74dacba4975f

D.3 Model-Level Optimizations

During initial experimental runs, we observed that CEM and the autoregressive CBM were substantially slower than Hard CBM. Inspecting the legacy implementation showed that both models evaluated many concept-specific modules sequentially in Python loops, creating avoidable model-forward overhead.

For CEM, the positive and negative concept embedding layers were implemented as many small per-concept modules. We replaced these repeated per-concept calls with batched linear projections while preserving the original positive/negative embedding scoring semantics. This reduces Python-loop overhead and allows the concept embeddings for all concepts to be computed in a single batched tensor operation.

For the autoregressive CBM, the legacy implementation creates C separate concept predictors and evaluates them in a Python loop. During teacher-forced concept training, the input to the predictor for concept c_i is the intermediate representation together with the ground-truth previous concepts $c_1, \ldots, c_{i-1}$. Since these previous concepts are known during training, the concept predictors do not need to be evaluated sequentially. We therefore implemented a packed autoregressive concept predictor. Each concept-specific MLP is represented by a slice of a batched parameter tensor, and all predictors use a padded input of size $d + C$, where d is the dimension of the intermediate representation. A lower-triangular concept mask ensures that the predictor for concept c_i only receives the previous concepts $c_{<i}$, preserving the autoregressive conditioning structure. This allows all concept predictors to be evaluated in parallel using batched matrix multiplications, reducing Python-loop and repeated concatenation overhead during concept training. For stages that require sequential sampling from the autoregressive model, we retain a single-concept forward path, since later sampled concepts depend on earlier sampled concepts.

For SCBM, we reduced overhead in the covariance-related computations. We cached the triangular indices used to construct covariance factors, avoiding repeated index construction during training and intervention. We also replaced explicit matrix inversions in the precision-matrix regularization loss with triangular solves based on the Cholesky factor where applicable.

Finally, for sampling-based methods, we vectorized target prediction across Monte Carlo samples. Instead of iterating over samples in a Python loop, we reshape the sampled concept tensors and evaluate the target predictor in batched form. This optimization is used during both training and intervention evaluation.

D.4 Intervention Evaluation Optimizations

In the legacy implementation, intervention results are computed in a step-first order. First, the initial intervention tensors are collected through a full model pass over the test set. For each intervention step, the legacy implementation iterates over the full test set, materializes the updated intermediate tensors, and uses them to construct the input dataset for the next intervention step, which introduces substantial overhead because intermediate states are repeatedly materialized and transferred between CPU and GPU. We therefore implemented intervention in a batch-first order. After the same initial collection step, the optimized implementation processes one batch at a time and completes all intervention steps for that batch so that the relevant tensors remain on the GPU, therefore avoiding repeated dataset construction and unnecessary CPU–GPU transfers of intermediate states.

D.5 Fast Intervention Solver

The dependency-aware intervention strategy in Section 3.2 requires solving a constrained optimization problem for the intervention logits $\boldsymbol{\eta}'_{\mathbb{S}}$. In the legacy implementation, this problem is solved independently for each sample using the SLSQP algorithm (Kraft, 1988) through SciPy (Virtanen et al., 2020) on the CPU. Although SLSQP provides a reliable solution, solving many small per-sample problems on the CPU prevents GPU-side vectorization and introduces repeated CPU–GPU data transfers.

To reduce this overhead, we implement a batched solver using the Frank-Wolfe algorithm (Frank & Wolfe, 1956) in PyTorch. The solver keeps the same optimization objective and constraints, but reparameterizes the intervention logits as

$$\boldsymbol{\eta}'_{\mathbb{S}} = \boldsymbol{\mu}_{\mathbb{S}} + \boldsymbol{s} \odot \boldsymbol{u}, \qquad s_i = 2c_i - 1, \qquad u_i \geq 0,$$

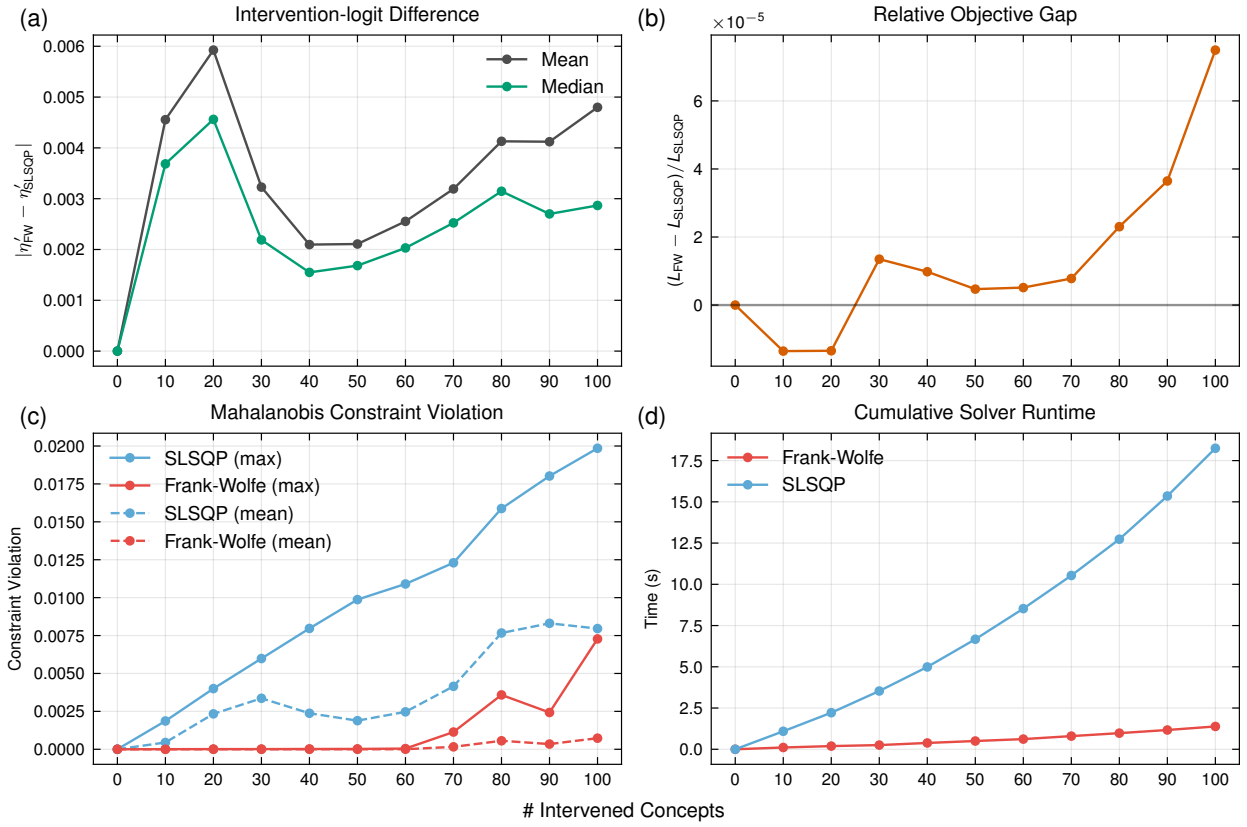

Figure 4: Validation of the Frank-Wolfe solver against SLSQP on 512 samples with 100 concepts. **(a)** Mean and median absolute differences between the intervention logits η' produced by the two solvers. **(b)** Relative objective gap $(L_{\mathrm{FW}} - L_{\mathrm{SLSQP}})/|L_{\mathrm{SLSQP}}|$, where positive values indicate that Frank-Wolfe achieves a worse objective than SLSQP. **(c)** Mean and maximum Mahalanobis-distance constraint violations for Frank-Wolfe and SLSQP separately; lower is better. **(d)** Cumulative solver runtime as more concepts are intervened, summed over all samples in the batch.

where $\odot$ denotes elementwise multiplication, and c_i is the known concept value for concept i. This reparameterization converts the direction constraints into non-negativity constraints. The Mahalanobis-distance constraint remains a positive-definite quadratic constraint in the new variable $\boldsymbol{u}$:

$$\boldsymbol{u}^\top \boldsymbol{A}\boldsymbol{u} \le \chi^2_{|\mathbb{S}|,0.99}, \qquad \boldsymbol{A} = \mathrm{diag}(\boldsymbol{s})\boldsymbol{\Sigma}^{-1}_{\mathbb{S},\mathbb{S}}\mathrm{diag}(\boldsymbol{s}).$$

Together with $\boldsymbol{u} \ge \boldsymbol{0}$, the feasible set is the intersection of this ellipsoid with the non-negative orthant.

For the ellipsoidal part of the feasible set, the Frank-Wolfe linear minimization direction has a closed-form solution proportional to $-\boldsymbol{A}^{-1}\boldsymbol{g}$, where $\boldsymbol{g}$ is the current gradient of the objective with respect to $\boldsymbol{u}$. Our implementation computes this direction in batch, clamps negative coordinates to satisfy the direction constraint, and rescales the result to the Mahalanobis-distance boundary. This yields a GPU-vectorized approximate solver for the constrained optimization problem.

We validate the Frank-Wolfe solver against the SLSQP solver on a batch of 512 synthetic samples with 100 concepts. Figure 4 reports the validation results. The mean absolute difference in intervention logits remains on the order of 10^{-3} across all numbers of intervened concepts, indicating that the two solvers produce numerically close solutions. Although the relative objective gap becomes slightly positive at larger intervention sizes, it remains on the order of 10^{-5}, suggesting comparable optimization quality. For constraint satisfaction, Frank-Wolfe achieves lower mean and maximum Mahalanobis-distance violations than SLSQP across all settings, indicating that the constraint is better respected by the Frank-Wolfe solver in this benchmark.

Finally, Frank-Wolfe substantially reduces cumulative runtime compared to SLSQP. Together, these results support using Frank-Wolfe as a practical replacement for SLSQP in large-scale intervention evaluation.

D.6 Timing Benchmarks

In Table 4, we compare the runtime of the legacy and optimized implementations. All timings are measured on a single GeForce RTX 4090, thereby isolating the effect of our implementation changes. The benchmarks are reported by dataset, model, and stage, following the same experimental settings described for Table 2.

Table 4: Timing comparison between the legacy and optimized implementations.

Dataset	Model	Stage	Legacy (s)	Optimized (s)	Speedup
Synthetic	Autoregressive CBM	pretrain	49.7	2.9	17.1×
		concept	58.9	3.6	16.4×
		target	5.6	1.6	3.5×
		intervention	576.2	45.6	12.6×
	CEM	joint	86.9	4.7	18.5×
		intervention	62.7	37.2	1.7×
	Hard CBM	joint	30.2	4.8	6.3×
		intervention	63.0	38.4	1.6×
	Amortized SCBM	joint	16.2	11.1	1.5×
		intervention	108.5	55.8	1.9×
	Global SCBM	joint	14.2	9.5	1.5×
		intervention	134.6	55.6	2.4×
CUB	Autoregressive CBM	pretrain	43.8	8.6	5.1×
		concept	52.4	13.9	3.8×
		target	20.6	1.3	15.8×
		intervention	753.9	44.7	16.9×
	CEM	joint	67.3	15.5	4.3×
		intervention	110.3	34.7	3.2×
	Hard CBM	joint	36.0	15.6	2.3×
		intervention	107.6	36.2	3.0×
	Amortized SCBM	joint	23.7	17.8	1.3×
		intervention	154.3	60.9	2.5×
	Global SCBM	joint	20.2	16.4	1.2×
		intervention	229.0	61.8	3.7×
CIFAR-10	Autoregressive CBM	pretrain	188.2	8.7	21.6×
		concept	198.4	11.4	17.4×
		target	111.8	3.6	31.1×
		intervention	1264.6	86.1	14.7×
	CEM	joint	263.3	12.6	20.9×
		intervention	185.5	74.5	2.5×
	Hard CBM	joint	112.8	14.0	8.1×
		intervention	193.3	73.3	2.6×
	Amortized SCBM	joint	120.2	29.3	4.1×
		intervention	278.4	104.8	2.7×
	Global SCBM	joint	124.6	27.5	4.5×
		intervention	504.8	104.2	4.8×